This CVPR paper is the Open Access version, provided by the Computer Vision Foundation.
Except for this watermark, it is identical to the accepted version;
the final published version of the proceedings is available on IEEE Xplore.

Spectral Informed Mamba for Robust Point Cloud Processing

Ali Bahri * Moslem Yazdanpanah Mehrdad Noori Sahar Dastani
Milad Cheraghalikhani Gustavo Adolfo Vargas Hakim David Osowiechi
Farzad Beizaee Ismail Ben Ayed Christian Desrosiers

LIVIA, ÉTS Montréal, Canada
International Laboratory on Learning Systems (ILLS)

Abstract

State Space Models (SSMs) have shown significant promise in Natural Language Processing (NLP) and, more recently, computer vision. This paper introduces a new methodology that leverages Mamba and Masked Autoencoder (MAE) networks for point-cloud data in both supervised and self-supervised learning. We propose three key contributions to enhance Mamba's capability in processing complex point-cloud structures. First, we exploit the spectrum of a graph Laplacian to capture patch connectivity, defining an isometry-invariant traversal order that is robust to viewpoints and captures shape manifolds better than traditional 3D grid-based traversals. Second, we adapt segmentation via a recursive patch partitioning strategy informed by Laplacian spectral components, allowing finer integration and segment analysis. Third, we address token placement in MAE for Mamba by restoring tokens to their original positions, which preserves essential order and improves learning. Extensive experiments demonstrate the improvements that our approach brings over state-of-the-art baselines in classification, segmentation, and few-shot tasks. The implementation is available at: https://github.com/AliBahri94/SI-Mamba.git.

1. Introduction

The analysis of 3D point cloud data is fundamental for various applications, including autonomous driving [36, 41], VR/AR [18], and robotics [39]. Compared to the organized structure of 2D images, point clouds consist of 3D coordinates without direct adjacency information forming an unordered bag. In recent years, considerable efforts have been dedicated to adapt deep learning models such as convolutional neural networks (CNNs) and Transformers to this type of data [2, 3, 32, 35, 54, 55]. Due to their permutation-invariant self-attention mechanism, Transformer networks

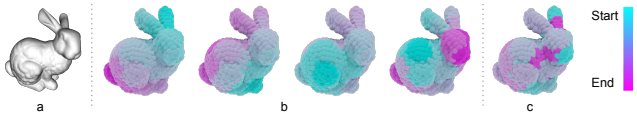


Figure 1. (a) Surface-Aware Spectral Traversing (SAST) applied to the patched point clouds of a mesh surface. (b) Traversal from left to right, based on the first to fourth non-constant smallest eigenvectors. (c) Traversal based on the largest eigenvector, forming a non-continuous sequence of tokens.

are particularly well suited for the unordered nature of point clouds. However, the quadratic complexity of this mechanism, requiring the computation of a weight between each pair of tokens, impedes the application of these networks to large-sized inputs (e.g., 2D images or 3D point clouds represented by many patches). This has prompted researchers to explore more efficient solutions, including the Set Transformer [24], Sparse Transformer [7], Longformer [4] and Sinkhorn Transformer [43].

Recently, methods based on Structured State Space Sequence (S4) [16] such as Mamba [14] have gained significant traction as a more efficient alternative to Transformers [29, 60]. So far, very few studies have investigated the potential of S4 approaches such as Mamba for 3D point clouds. Existing methods like Point-Mamba [26] and PCM [57] extend the 2D grid-based traversal used for images to a 3D grid. However, this straightforward adaptation to point clouds suffers from three crucial problems. **First:** whereas patches from 2D images have adjacency information, which could be exploited by the grid-based traversal, the 3D point patches in point clouds offer a sparse representation of the object's surface, and nearby patches on a 3D grid are not necessarily adjacent on this surface. **Second:** in the absence of self-attention, task-specific performance is highly influenced by the nature of the token traversal strategy. For example, a traversal suitable for point cloud classification may not be effective for a local task such as point-level classification (i.e., segmentation). **Third:** due to the "direction-sensitive" nature of Mamba, the self-supervised MAE pre-

*Correspondence to ali.bahri.1@ens.etsmtl.ca

training step of leading point cloud models like Point-MAE [32] and Point-M2AE [55] cannot be used directly as there is no attention mechanism to learn the masked tokens' positions.

The contribution of our work focuses on addressing these problems as follows:

1. We introduce a Surface-Aware Spectral Traversing (SAST) strategy based on the Laplacian spectrum of a patch-connectivity graph. Compared to the 3D grid traversal of current approaches like Point-Mamba, our strategy is invariant to isometric transformations (e.g., choice of viewpoint) and better captures the object's surface manifold.
2. We also present a Hierarchical Local Traversing (HLT) for point-level classification (segmentation) that partitions patches recursively based on their spectral coordinates. Unlike our SAST strategy for classification, which considers Laplacian eigenvectors separately in different traversals, this HLT combines them in a single ordering for a more precise modeling of geometry.
3. During the MAE-based Self-Supervised Learning (SSL), we propose a Traverse-Aware Repositioning (TAR) strategy to align the masked tokens according to their spectral adjacency. This strategy addresses the critical issue of spatial adjacency preservation unique to Mamba networks.

2. Related Works

Deep Point Cloud Learning. Deep neural networks have increasingly been applied to point clouds, with early architectures like PointNet [34] and PointNet++ [35] inspiring further work [1, 10, 23, 25, 58] focused on capturing local context. Transformer-based frameworks [46], including the Point Transformer (v1–v3) [50, 51, 59] and Stratified Transformer [22], have set new benchmarks by integrating both local and global features. Recently, self-supervised pre-training has gained traction by leveraging masked point modeling [28, 42] to train Transformers on unlabeled data.

Building on the effectiveness of MAE in Text and Image domains, Point-BERT [54] presented a revolutionary method inspired by BERT [11], tailoring Transformers to 3D point cloud processing. Point-MAE [32] applied MAE-style pre-training to 3D point clouds using a custom Transformer-based Autoencoder (AE) designed to reconstruct masked irregular patches. The use of multi-scale masking and local spatial self-attention mechanisms in Point-M2AE [55] has led to State-Of-The-Art (SOTA) results in 3D representation learning. Furthermore, I2P-MAE [56] improved self-supervised point cloud processing with a masking strategy leveraging pre-trained 2D models through an Image-to-Point transformation. Point-GPT [6] introduced an auto-regressive generative pretraining (GPT) approach to address the unordered nature and low information density of point clouds. ACT [12] proposed a cross-modal knowledge transfer method using pretrained 2D or natural language Transformers as teachers for 3D representation learning. Finally, GeoMask3D [2] is a self-supervised point cloud method that uses a teacher-student model to select harder, geometrically intricate regions for masking, thereby improving feature representations.

2.1. State Space Models

State Space Models. State-space models (SSMs) have been foundational in control theory and signal processing for modeling dynamic systems. Recently, they have been adapted to deep learning, with advancements like the Linear State-Space Layer (LSSL), which uses a continuous-time memorization framework based on the HiPPO operator [15] to model long-range dependencies. However, LSSL's high computational demands limit its practicality. To address this, the S4 model [16] introduced parameter normalization techniques, paving the way for structured SSMs with enhancements like complex-diagonal structures [17, 19], support for multiple-input/output [17], and low-rank decomposition [20]. Recent developments include Mamba [14], which achieves linear-time inference and efficient training through selection mechanisms and hardware-aware algorithms. MoE-Mamba further boosts efficiency by integrating a Mixture of Experts (MoE), outperforming both Mamba and Transformer-MoE models [33].

SSMs for Vision Tasks The above-mentioned works primarily focused on the application of SSMs to long-range or causal data types such as language and speech. In the field of vision, a notable study [29] proposed the VMamba model which features a Cross-Scan Module (CSM) for enhanced 1D selective scanning in 2D spaces and architectural optimizations that significantly improve its performance and speed across various visual tasks. Another significant paper is Vision Mamba [60] which introduces a novel vision backbone called Vim utilizing bidirectional Mamba blocks.

For point cloud analysis based on Mamba, two key works are Point-Mamba [26] and PCM [57]. PointMamba introduces a simple approach to token reordering for point cloud analysis by strategically organizing point tokens based on a 3D grid. Similarly, PCM enhances Mamba with a Consistent Traverse Serialization (CTS) technique that converts 3D point clouds into 1D point sequences while maintaining spatial adjacency. Building upon these approaches, our method introduces the Spectral Spatial Traversing (SST) strategy, which improves token ordering and maintains spatial adjacency within Mamba networks.

3. Method

We begin by outlining the fundamental concepts of SSMs and spectral graph analysis which are at the core of our

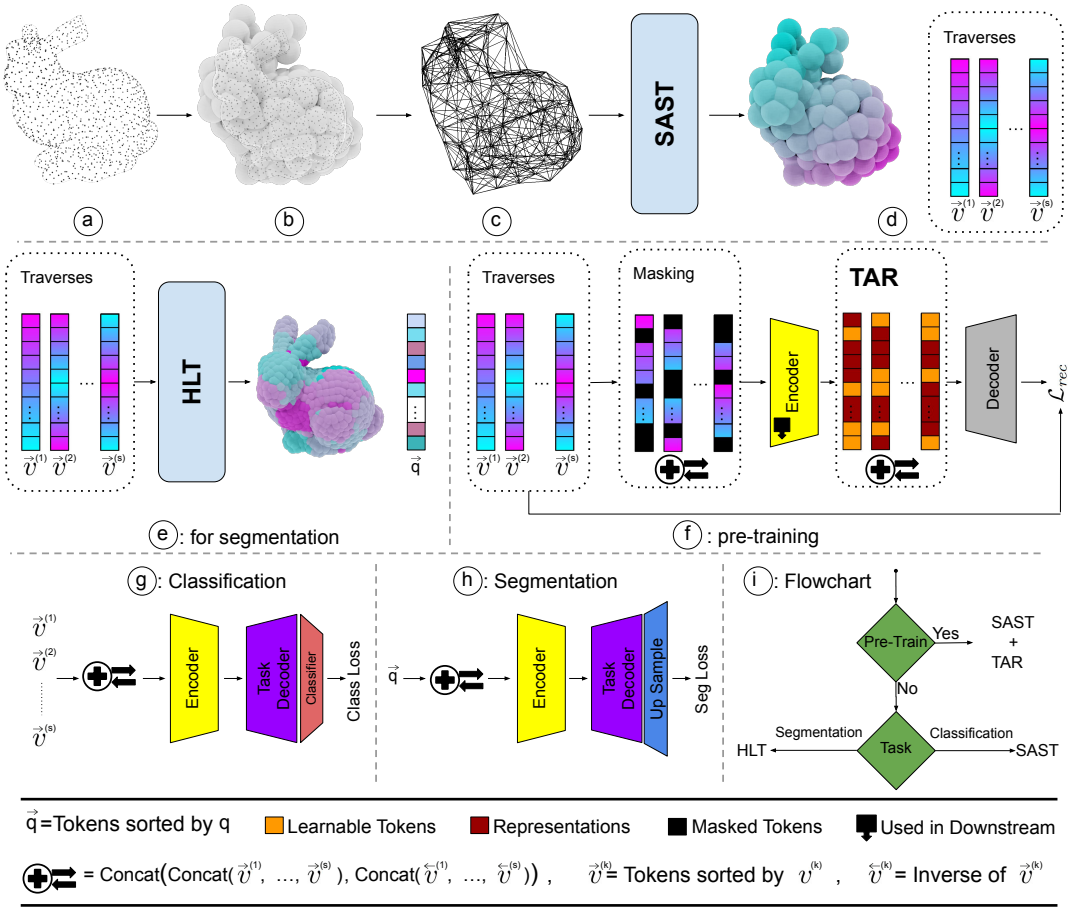


Figure 2. Overview of the proposed Spectral Spatial Traversing (SST) method. (a) Point cloud, (b) Patchification, (c) Forming the adjacency graph, (d) Traversal based on SAST using s non-constant smallest eigenvectors, (e) HLT for segmentation tasks, (f) TAR strategy for Masked Autoencoders. The process includes reverse and concatenation operations, with learnable tokens, representations, and masked tokens highlighted. (g) The classification task involves sorting tokens by different eigenvectors, concatenating them, and then feeding them into the network. (h) The segmentation task where HLT is applied on the tokens ($\vec{q}$) and $\vec{q}$ is fed into the network. (i) A flowchart visualizing the techniques used in self-supervised learning and various downstream tasks.

work. We then give an in-depth presentation of our Surface-Aware Spectral Traversing (SAST) strategy for point cloud processing that improves the model's robustness to isometric transformations and better captures the underlying manifold of the point cloud. Thereafter, we provide detailed specifications of our Hierarchical Local Traversing (HLT) strategy for point-level classification, which defines a more structured patch traversal order based on the recursive partitioning of spectral information. Finally, we introduce our Traverse-Aware Repositioning (TAR), which improves the handling of learnable tokens in masked autoencoders within Mamba networks. Fig. 2 illustrates the overview of the proposed Spectral Spatial Traversing (SST) method.

3.1. Preliminaries

State Space Models (SSMs) use a series of first-order differential equations to describe how the state of the linear, time-invariant system evolves over time:

$$\dot{h}(t) = Ah(t) + Bx(t), \quad y(t) = C\dot{h}(t) + Dx(t), \quad (1)$$

Here, $\dot{h}(t)$ denotes the time derivative of the state vector $h(t)$. The matrices A, B, C, and D are the weighting parameters.

Due to their reliance on continuous data streams $x(t)$, SSMs are not natively equipped to handle discrete inputs represented as $\{x_0, x_1, \ldots\}$. This necessitates the use of a discretized SSM version for practical applications:

$$h_k = \bar{A}h_{k-1} + \bar{B}x_k, \quad y_k = \bar{C}h_k + \bar{D}x_k. \quad (2)$$

The state space model in its discrete version utilizes a recursive function to link each state h_k to its preceding state, encapsulated by the matrices $\bar{A} \in \mathbb{R}^{N\times N}$, $\bar{B} \in \mathbb{R}^{N\times 1}$, and $\bar{C} \in \mathbb{R}^{N\times 1}$, which are tuned parameter matrices. While

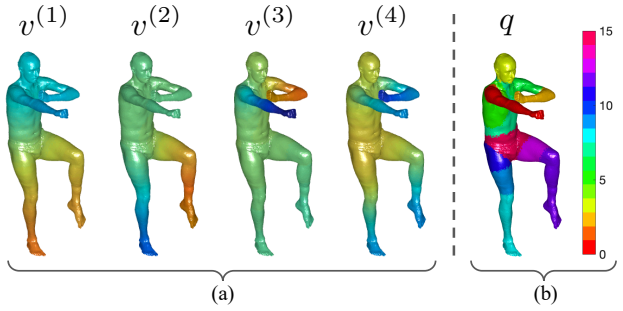


Figure 3. (a) Visualization of the four non-constant smallest Laplacian eigenvectors ($v^{(k)}$, $k = 1, \ldots, 4$) and (b) the discrete partitioning (q) of our HLT strategy combining the information of all four eigenvectors. Note: we assumed that patches contain a single point for better visualization.

matrix $\bar{D} \in \mathbb{R}^{N\times 1}$ may be employed as a residual connection, we follow previous work and exclude it from our model. The transition from a continuous signal representation $x(t)$ to a discrete sequence involves sampling $x(t)$ at intervals defined by Δ, setting each discrete input as $x_k = x(k\Delta)$. This adjustment to a discrete framework results in revised matrix definitions:

$$\bar{A} = (I - \frac{\Delta}{2}A)^{-1}(I + \frac{\Delta}{2}A), \bar{B} = (I - \frac{\Delta}{2}A)^{-1}\Delta B, \bar{C} = C. \tag{3}$$

However, the fixed dynamics of Linear Time-Invariant (LTI) models, exemplified by the constant parameters A, B, and C in Eq. (3), restrict their capacity to selectively retain or discard relevant information, thereby limiting their contextual awareness. To improve content-aware reasoning, we use Mamba's selection mechanism that manages the propagation and interaction of information across the sequence dimension [14].

Spectral Graph Analysis. Popularized by Chung in the 90s [8], spectral graph analysis characterizes the properties of a graph $G = (V, E)$ by the spectrum (eigenvalues and corresponding eigenvectors) of its Laplacian matrix L. This analysis can be understood as a discretized version of the Laplace-Beltrami Operator Δ of a function f defined on a Riemannian manifold:

$$\Delta f = \mathrm{div}(\mathrm{grad} f) \tag{4}$$

where $\mathrm{grad} f$ is the gradient of f and div the divergence on the manifold. The solution to the Laplacian eigenvalue problem $\Delta f = -\lambda f$, known as Helmholtz wave equation, is an eigenfunction corresponding to the natural vibration form of a homogeneous membrane with eigenvalue λ [38].

Following methods for spectral clustering [31] and normalized cuts [40], we consider a weighted adjacency matrix $W : V \times V \to \mathbb{R}_+$ where $W_{ij} = 0$ if $(i, j) \notin E$ to model the Euclidean distance of nearby patches (see Section 3.3). The Laplacian matrix of G is defined as $L = D - W$ where D is the diagonal *degree* matrix such that $D_{ii} = \sum_j W_{ij}$. To account for variability in the scale of weights W_{ij} or the distribution of node degrees D_{ii}, it is preferable to employ a normalized version of the Laplacian. In this work, we use the Random Walk Laplacian $L_{rw} = I - D^{-1}W$ which has the following useful properties:

1. L_{rw} is positive semi-definite and has $|V|$ non-negative real-valued eigenvalues $0 = \lambda_1 \leq \ldots \leq \lambda_{|V|}$;
2. 0 is an eigenvalue of L_{rw} with the constant vector as eigenvector and its multiplicity equals the number of connected components in the graph;
3. Following Courant's Nodal Line Theorem [9], the n-th eigenmode of L_{rw} has at most n poles of vibration;
4. The representation of a shape by the spectrum of L_{rw} is invariant to isometry (i.e., distance-preserving transformation).

Our method uses the s first non-constant eigenvectors of L_{rw} (i.e., the eigenvectors corresponding to the s smallest non-zero eigenvalues) to define traversal orders for classification (Section 3.3) and segmentation (Section 3.4) that are robust to the viewpoint (due to isometry invariance) and provide a smooth parametrization of the surface manifold. We consider the first eigenvectors as they encode low frequency information (by Courant's Nodal Line Theorem), making the resulting traversal more robust to shape variability and noise. Fig. 1 illustrates this concept: (a) shows the original mesh, (b) shows traversals based on the first to fourth non-constant smallest eigenvectors, and (c) shows traversal based on the largest eigenvector forming a non-continuous sequence of tokens.

3.2. Point Cloud Patchification

Given a point cloud $\mathcal{P} = \{p_i\}_{i=1}^{N_p}$, each point represented by 3D coordinates, we convert $\mathcal{P}$ to a reduced set of patches that can be processed more efficiently. Toward this goal, we employ the Farthest Point Sampling (FPS) algorithm to select a subset $\mathcal{C} \subset \mathcal{P}$ of N_c points offering a good coverage of the entire point cloud. These selected points will act as the centers of local patches within the point cloud. For each center point $p_{s_i} \in \mathcal{C}$, we then identify N_n nearest points $\mathcal{N}(p_{s_i}) \subset \mathcal{P}$ using the K-Nearest Neighbours (KNN) algorithm. Following this, each patch is defined as a center p_{s_i} and its corresponding nearest-neighbors $\mathcal{N}(p_{s_i})$.

3.3. Surface-Aware Spectral Traversing (SAST)

Current point cloud processing approaches using Mamba, such as Point-Mamba [26] and PCM [57], simply extend the 2D grid-based traversal for images to a 3D grid. As mentioned before, this naive strategy suffers from two issues: 1) the 3D grid is view dependent, thus rotating the point cloud or moving the camera yields a different traversal order; 2) unrelated patches may be adjacent in 3D space, hence can be traversed subsequently. To address these problems, we

define a traversal order based on the Laplacian spectrum of the patch-connectivity graph.

In this graph, each node corresponds to a patch and the weighted adjacency matrix W is defined using the Euclidean distance between patch centers. For patches i and j defined by center points p_{s_i} and p_{s_j}, we add an edge (i, j) if p_{s_j} is among the K nearest neighbors of p_{s_i} or vice-versa. The weight of this edge is computed using a Gaussian kernel: $W_{ij} = \exp\left(-\|p_{s_i} - p_{s_j}\|_2^2/\sigma\right)$ where σ is a hyperparameter controlling the kernel width.

Following Section 3.1, we compute the s first non-constant eigenvectors of the Random Walk Laplacian L_{rw}. This can be achieved efficiently using an iterative method like the Arnoldi algorithm [13] by exploiting the following facts: 1) matrix W is very sparse, and 2) only the first few eigenvectors need to be computed. Eigenvector $v^{(k)} \in \mathbb{R}^{N_c}$, $k \in \{1, \dots, s\}$, assigns an eigenfunction value $v_i^{(k)}$ to each patch i. In each Mamba block of our model, we perform two separate traversals of tokens (each token corresponds to an input patch) for *every* eigenvector: a forward traversal by increasing value of $v_i^{(k)}$ and a reserve traversal by decreasing value of $v_i^{(k)}$. At the end of the block, we concatenate the tokens from the $s \times 2$ traversals. The visual effect of each traversal is illustrated in Fig. 1(b) and Fig. 3(a).

Canonicalization of spectrum. Although the spectrum of L_{rw} forms an isometry-invariant representation of the surface manifold, this representation may be impacted by two sources of ambiguity: 1) the sign of eigenvectors is undetermined (i.e., if $v^{(k)}$ is an eigenvector, then so is $-v^{(k)}$), and 2) the order of eigenvectors with similar eigenvalues may vary. We address these two sources of ambiguity with the following canonicalization procedure. For the first one, we flip the sign of an eigenvector $v^{(k)}$ (i.e., $v^{(k)} := -v^{(k)}$) if its first element is negative (i.e., $v_1^{(k)} < 0$). To handle the second ambiguity, we first sort the eigenvectors by non-decreasing eigenvalue. We deal with eigenvalues having a mutliplicity greater than one by finding pairs of consecutive eigenvectors $v^{(k)}$, $v^{(k+1)}$ with near-identical eigenvalues (i.e., $|\lambda_k - \lambda_{k+1}| \leq \epsilon$). For such pairs, we flip the order if $v_1^{(k)} > v_1^{(k+1)}$. This reordering process is repeated until no further change occurs.

3.4. Hierarchical Local Traversing (HLT) for Segmentation

While effective for classification tasks, the SAST strategy considering each eigenvector in a *separate* traversal may not capture the precise relationship between patches needed for segmentation. To address this issue, we introduce a Hierarchical Local Traversal (HLT) strategy that considers the full spectrum (all s non-constant eigenvectors) simultaneously.

Our strategy is inspired by the recursive binary partitioning technique of normalized cuts [40]. Starting from the canonicalized spectrum (see Section 3.3), tokens are first split based on the first eigenvector $v^{(1)}$, by comparing their corresponding value in $v^{(1)}$ with the mean value $\overline{v}^{(1)}$. This yields a binary partition of tokens $b_i^{(1)} = \mathbb{1}\big(v_i^{(1)} \geq \overline{v}^{(1)}\big) \in \{0, 1\}$ where $\mathbb{1}$ is the indicator function. Each subgroup is then divided based on the mean of the second eigenvector $v^{(2)}$, and so on for other eigenvectors. This partitioning process can be seen as building a binary tree, where each level corresponds to a different eigenvector and leaf nodes i are uniquely identified by the sequence of bits $b_i = [b_i^{(1)}, \dots, b_i^{(s)}]$ on the path from the root to the leaf. Our HLT method traverses groups of leaf nodes (groups of tokens) sequentially based on the lexicographic order of their binary code (e.g., [0000], [0001], [0010], [0011], ... in the case of four eigenvectors). For convenience, we convert binary codes b_i to a non-negative integer q_i (e.g., $bin2Int([0011]) = 3$) and define two traversal orders, by increasing or decreasing values of q_i.

For s eigenvectors, the HLT strategy described above divides tokens into 2^s segments which are traversed sequentially. In the best case scenario, $\lceil \log_2(N_c) \rceil$ eigenvectors are thus needed to split tokens into individual segments. However, it may happen that multiple tokens fall in the same segment, especially when using fewer eigenvectors. In such case, one can further sort tokens *within* each segment, for example, using the values of the first eigenvector (i.e., $v^{(1)}$). In our implementation, we simply sort these tokens randomly to add stochasticity in the training. This section is illustrated in Fig. 2 (e), and Fig. 3 (b).

As shown in Fig. 3, the first Laplacian eigenvectors encode high-level spatial relations (e.g., bottom *vs.* top, left *vs.* right, torso *vs.* limbs, etc.). In the SAST, because these eigenvectors are used in *separate* traversals, the network may not be able to differentiate specific regions/parts of the point cloud. In contrast, our HLT strategy can capture such specific parts (e.g., head, left or right arm/thigh/calf, pelvis, etc.).

3.5. Traverse-Aware Repositioning (TAR) for Masked Autoencoders

Following state-of-art Transformers for point cloud processing, such as Point-MAE [32] and Point-M2AE [55], our method leverages self-supervised pretraining based on MAE to boost performance. In Transformer-based approaches, the learnable tokens of masked patches can be inserted in any position of the sequence (typically at the end) as the self-attention mechanism can still attend to all tokens irrespective of their positions. However, this approach presents a significant problem in Mamba networks which are sensitive to the traversal order of tokens. We handle this problem via a TAR strategy that improves the placement of learnable tokens in MAE within Mamba networks. Specifically, we restore the learnable tokens to their

original positions rather than appending them at the end of the sequence. This ensures that the essential order of tokens is maintained, preserving spatial adjacency and enhancing learning effectiveness within Mamba networks.

The proposed TAR strategy selects an arbitrary traversal order and randomly masks a subset of N_m tokens with the same masking ratio as the transformer-based MAEs. These tokens are then removed from the sequence, and their positions are recorded. Afterwards, the remaining (visible) tokens are fed to the encoder that outputs their representation. Before reconstructing the point cloud using the decoder, we reinsert the learnable tokens in the sequence at their recorded position. The set of masked patches is used for other traversal orders. This procedure can be seen in Fig. 2 (f). Following previous work, we measure the reconstruction error for masked patches using the Chamfer distance:

$$\mathcal{L}_{rec} = \frac{1}{N_m} \sum_{i=1}^{N_m} \text{Chamfer}(\mathcal{S}_i, \hat{\mathcal{S}}_i), \tag{5}$$

where $\mathcal{S}_i \in \mathbb{R}^{N_n \times 3}$ is the set of points forming the i-th masked patch and $\hat{\mathcal{S}}_i$ the reconstructed output for these points. The Chamfer distance between two sets of points $\mathcal{S}$ and $\hat{\mathcal{S}}$ is defined as

$$\begin{aligned} \text{Chamfer}(\mathcal{S}, \mathcal{S}') = & \sum_{p \in \mathcal{S}} \min_{p' \in \mathcal{S}'} \|p - p'\|_2^2 \\ & + \sum_{p' \in \mathcal{S}'} \min_{p \in \mathcal{S}} \|p - p'\|_2^2. \end{aligned} \tag{6}$$

4. Experiments

Several experiments are conducted to evaluate the proposed method. First, we pretrain the Point-Mamba network using our techniques on the ShapeNet [5] training dataset. We then assess the performance of these pretrained models across a variety of standard benchmarks, including object classification, few-shot learning, and segmentation. Additionally, we train the model from scratch on downstream datasets to demonstrate the robustness and versatility of our method. To have a fair comparison, we adopt the masking ratio (60%) that was used in the Point-Mamba model. Moreover, a comprehensive analysis of the computational efficiency, runtime, and memory usage of our SAST approach is provided in the Supplementary Material.

Table 1. **Few-shot classification on ModelNet40**. We report the average accuracy (%) and standard deviation (%) of 10 independent experiments. '*' denotes reproduced results. A^{std} represents the average (A) and standard deviation (std), respectively.

Method	5-way		10-way	
	10-shot	20-shot	10-shot	20-shot
DGCNN [48]	$91.8^{3.7}$	$93.4^{3.2}$	$86.3^{6.2}$	$90.9^{5.1}$
DGCNN + OcCo [47]	$91.9^{3.3}$	$93.9^{3.1}$	$86.4^{5.4}$	$91.3^{4.6}$
Transformer [54]	$87.8^{5.2}$	$93.3^{4.3}$	$84.6^{5.5}$	$89.4^{6.3}$
Transf. + OcCo [54]	$94.0^{3.6}$	$95.9^{2.3}$	$89.4^{5.1}$	$92.4^{4.6}$
Point-BERT [54]	$94.6^{3.1}$	$96.3^{2.7}$	$91.0^{5.4}$	$92.7^{5.1}$
Point-M2AE [55]	$96.8^{1.8}$	$98.3^{1.4}$	$92.3^{4.5}$	$95.0^{3.0}$
Point-MAE [32]	$96.3^{2.5}$	$97.8^{1.8}$	$92.6^{4.1}$	$95.0^{3.0}$
PointMamba* [26]	$95.9^{2.1}$	$97.3^{1.9}$	$91.6^{5.3}$	$94.5^{3.5}$
Ours	$\mathbf{96.4}^{2.1}$	$\mathbf{98.5}^{1.5}$	$\mathbf{92.0}^{5.1}$	$\mathbf{95.1}^{3.6}$

4.1. Pretraining Setup

Following Point-Mamba, we adopt the ShapeNet [5] dataset for the pretraining and assess the quality of the 3D representations produced by our approach through a linear evaluation on the ModelNet40 [52] dataset. The linear evaluation is performed by a Support Vector Machine (SVM) fitted on these features. This classification performance is quantified by the accuracy metric. Augmentation in pretraining is *scale and transform*, while in finetuning it is *rotation*.

4.2. Downstream Tasks

Object Classification on Real-World Dataset. To evaluate our method for point clouds, we test it on the ScanObjectNN dataset [44], as described in previous studies. The augmentation used during training is random rotation. The results, presented in Tab. 3, show that our strategy signifi-

Table 2. **Part segmentation on the ShapeNetPart [53]**. The mIoU for all instances (Inst.) is reported. HLT is Hierarchical Local Traversing for segmentation.

Methods	Backbone	FLOPs (G)	mIoU
Training from scratch			
PointNet [34]	-	-	83.7
PointNet++ [35]	-	-	85.1
DGCNN [48]	-	-	85.2
APES [49]	-	-	85.8
Point-MAE [32]	Transformer	15.5	85.7
PointMamba [26]	Mamba	14.3	85.8
Ours (HLT)	Mamba	14.3	**85.9**
Training from pretrained			
Transformer [54]	Transformer	15.5	85.1
Point-BERT [54]	Transformer	15.5	85.6
Point-MAE [32]	Transformer	15.5	86.1
Point-M2AE [55]	Transformer	15.5	86.5
Point-GPT-S [6]	Transformer	-	86.2
ACT [12]	Transformer	-	86.2
I2P-MAE [56]	Transformer	-	86.8
PointMamba [26]	Mamba	14.3	86.0
Ours (SAST)	Mamba	14.3	85.7
Ours (HLT)	Mamba	14.3	**86.1**

Table 3. **Object classification on ScanObjectNN [45].** Accuracy (%) is reported. † indicates that this method was fine-tuned without rotation augmentation.

Methods	Backbone	Param. (M)	FLOPs (G)	OBJ-BG	OBJ-ONLY	PB-T50-RS	ModelNet40
Training from scratch							
PointNet [34]	-	3.5	0.5	73.3	79.2	68.0	89.2
PointNet++ [35]	-	1.5	1.7	82.3	84.3	77.9	90.7
DGCNN [48]	-	1.8	2.4	82.8	86.2	78.1	92.9
PointNeXt [37]	-	1.4	1.6	-	-	87.7	92.9
PointMLP [30]	-	13.2	31.4	-	-	85.4	-
ADS [21]	-	-	-	-	-	87.5	-
Transformer [54]	Transformer	22.1	4.8	79.86	80.55	77.24	-
Point-MAE [32]	Transformer	22.1	4.8	86.75	86.92	80.78	92.3
PointMamba [26]	Mamba	12.3	3.6	90.87	90.18	85.60	92.4
Ours	Mamba	12.3	3.6	**92.25**	**91.39**	**87.30**	**92.7**
Training from pretrained							
Transformer [54]	Transformer	22.1	4.8	79.86	80.55	77.24	92.1
Transformer-OcCo [54]	Transformer	-	-	84.85	85.54	78.79	-
Point-BERT [54]	Transformer	22.1	4.8	87.43	88.12	83.07	92.7
Point-M2AE† [55]	Transformer	-	-	91.22	88.81	86.43	94.0
Point-MAE [32]	Transformer	22.1	4.8	92.77	91.22	89.04	93.2
PointMamba [26]	Mamba	12.3	3.6	93.29	91.56	88.17	92.8
PCM [57]	Mamba	12.3	3.6	-	-	86.9	-
Ours	Mamba	12.3	3.6	**94.32**	**91.91**	**89.10**	**93.4**

cantly improves object classification accuracy in both training from scratch and fine-tuning scenarios. These findings highlight the effectiveness of our approach in enhancing the model's ability to identify and classify objects across various backgrounds, demonstrating its robustness in complex real-world scenarios.

Object Classification on Clean Objects Dataset. We also evaluated our method on the ModelNet40 [52] dataset, following the protocols established in previous works. The augmentation used during training is scale and transform. As shown in Tab. 3, our approach achieves notable enhancements on this challenging dataset compared to both the original Point-Mamba and the Transformer-based Point-MAE. This demonstrates the robustness and effectiveness of our method when applied to the Point-Mamba network.

Few-shot Learning. We conducted few-shot learning experiments on ModelNet40 [52] dataset, adhering to the protocols of previous studies [27, 32, 55]. The results of our few-shot learning experiments are presented in Tab. 1. Despite the competitive nature of this benchmark, our method demonstrated outstanding performance across all tested scenarios. As shown in Tab. 1, our Mamba-based method achieves results comparable to or exceeding those of transformer-based methods (Point-MAE and Point-M2AE).

Part Segmentation. We evaluated our method's representation learning ability on the ShapeNetPart dataset [53] using standard experimental settings [34, 35, 54]. Tab. 2 shows that performance gains in prior methods are minimal, highlighting the dataset's challenge. For instance, Point-GPT [6] and ACT [12], despite being state-of-the-art and complex methods, show only marginal improvements over each other and other state-of-the-art approaches. Similarly, I2P-MAE [56], which combines 3D data with 2D information, shows limited improvement over Point-M2AE. For the "Training from scratch" setting, our method outperforms several state-of-the-art approaches. In the "Training from pretrained" setting, we further demonstrate the effectiveness of HLT strategy compared to SAST in the segmentation task.

4.3. Ablation Studies

In this section, we aim to investigate the effects of different parameters on our method. We will focus on two key aspects: the effect of the number of non-constant smallest eigenvectors and the adjacency matrix used in the SAST strategy, and the analysis of the TAR strategy.

Analysis of Eigenvectors and Graph. One of our ablation studies investigates the impact of the number of non-constant smallest eigenvectors used in the SAST and TAR strategies. As depicted in Fig. 4 (*Left*), the best performance is achieved when using the four non-constant smallest eigenvectors (blue line) for traversing. When the num-

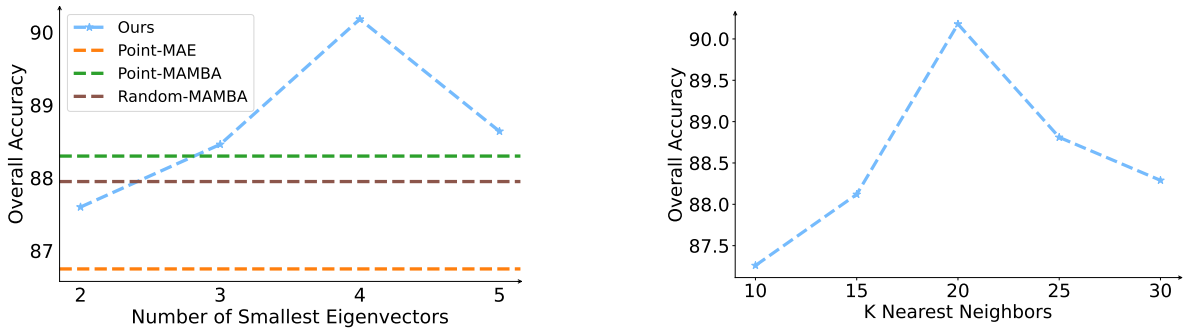


Figure 4. Analysis of the number of non-constant smallest eigenvectors and comparison with previous methods (*Left*) and analysis of the number of nearest neighbors K (*Right*).

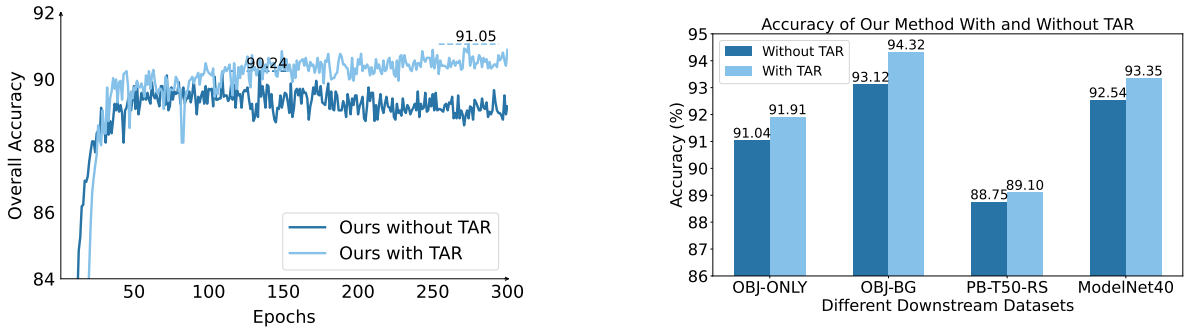


Figure 5. The effect of the TAR strategy in the pretraining phase (*Left*) and in finetuning (*Right*).

ber of non-constant smallest eigenvectors increases beyond four, the performance drops. This is because the additional eigenvectors are closer to the largest eigenvectors, which are less smooth and do not capture the most significant structural variations effectively. The significantly lower performance of Point-MAE [32], Point-Mamba [26], and Point-Mamba with random traversing (Random-Mamba) compared to ours underscores the importance of appropriate traversing for Mamba networks.

Another study examines the impact of the number of nearest neighbors used in creating the adjacency matrix. As shown in Fig. 4 (*Right*), the best performance (blue line) is achieved with 20 nearest neighbors. The model's accuracy increases as the number of nearest neighbors increases from 10 to 20, reaching its peak at 20 nearest neighbors. Beyond this point, the performance starts to decline. All these experiments are trained and evaluated from scratch on the ScanObjectNN dataset [44] (OBJ-BG) with *scale and transform* augmentation.

Analysis of TAR Strategy. One of the studies examines the impact of the TAR strategy on the model's performance. As shown in Fig. 5 (*Left*), the accuracy of the model with and without the TAR strategy is plotted against the number of epochs. The model incorporating the TAR strategy (light blue line) demonstrates superior performance compared to the model without TAR (dark blue line). This figure relates to the pretraining phase on the ShapeNet [5] dataset, which is subsequently tested on the ModelNet [52] dataset using a SVM.

Additionally, we evaluate the effect of the TAR strategy by fine-tuning pretrained models (with or without TAR) on four downstream tasks, each corresponding to a distinct dataset. As shown in Fig. 5 (*Right*), the model pretrained with TAR (light blue line) consistently achieves higher accuracy than the model trained without TAR (dark blue line). This demonstrates that the model pretrained with the TAR strategy has learned more meaningful features, leading to better performance in the downstream tasks.

5. Conclusion and Limitation

We introduced three strategies to enhance Mamba networks for point cloud data: isometry-invariant token traversal, recursive patch partitioning for segmentation, and improved learnable token placement, each contributing to a robust feature extraction framework. Our methods demonstrate superior performance over state-of-the-art baselines in classification, segmentation, and few-shot tasks. A limitation of our approach lies in the selection of the neighborhood size K, which is treated as a hyperparameter. While tuning K per dataset helps optimize performance, it may limit generalizability across diverse data distributions and require careful adjustment to maintain robustness.

References

[1] Matan Atzmon, Haggai Maron, and Yaron Lipman. Point convolutional neural networks by extension operators. *arXiv preprint arXiv:1803.10091*, 2018. 2

[2] Ali Bahri, Moslem Yazdanpanah, Mehrdad Noori, Milad Cheraghalikhani, Gustavo Adolfo Vargas Hakim, David Osowiechi, Farzad Beizaee, Ismail Ben Ayed, and Christian Desrosiers. Geomask3d: Geometrically informed mask selection for self-supervised point cloud learning in 3d. *arXiv preprint arXiv:2405.12419*, 2024. 1, 2

[3] Ali Bahri, Moslem Yazdanpanah, Mehrdad Noori, Sahar Dastani, Milad Cheraghalikhani, David Osowiech, Farzad Beizaee, Ismail Ben Ayed, Christian Desrosiers, et al. Test-time adaptation in point clouds: Leveraging sampling variation with weight averaging. *arXiv preprint arXiv:2411.01116*, 2024. 1

[4] Iz Beltagy, Matthew E Peters, and Arman Cohan. Longformer: The long-document transformer. *arXiv preprint arXiv:2004.05150*, 2020. 1

[5] Angel X Chang, Thomas Funkhouser, Leonidas Guibas, Pat Hanrahan, Qixing Huang, Zimo Li, Silvio Savarese, Manolis Savva, Shuran Song, Hao Su, et al. Shapenet: An information-rich 3d model repository. *arXiv preprint arXiv:1512.03012*, 2015. 6, 8

[6] Guangyan Chen, Meiling Wang, Yi Yang, Kai Yu, Li Yuan, and Yufeng Yue. PointGPT: Auto-regressively generative pre-training from point clouds. *Advances in Neural Information Processing Systems*, 36, 2024. 2, 6, 7

[7] Rewon Child, Scott Gray, Alec Radford, and Ilya Sutskever. Generating long sequences with sparse transformers. *arXiv preprint arXiv:1904.10509*, 2019. 1

[8] Fan RK Chung. *Spectral graph theory*. American Mathematical Soc., 1997. 4

[9] Richard Courant and David Hilbert. *Methods of mathematical physics: partial differential equations*. John Wiley & Sons, 2008. 4

[10] Xin Deng, WenYu Zhang, Qing Ding, and XinMing Zhang. Pointvector: a vector representation in point cloud analysis. In *Proceedings of the IEEE/CVF Conference on Computer Vision and Pattern Recognition*, pages 9455–9465, 2023. 2

[11] Jacob Devlin, Ming-Wei Chang, Kenton Lee, and Kristina Toutanova. Bert: Pre-training of deep bidirectional transformers for language understanding. *arXiv preprint arXiv:1810.04805*, 2018. 2

[12] Runpei Dong, Zekun Qi, Linfeng Zhang, Junbo Zhang, Jianjian Sun, Zheng Ge, Li Yi, and Kaisheng Ma. Autoencoders as cross-modal teachers: Can pretrained 2D image transformers help 3D representation learning? *arXiv preprint arXiv:2212.08320*, 2022. 2, 6, 7

[13] Gene H Golub and Charles F Van Loan. *Matrix computations*. JHU press, 2013. 5

[14] Albert Gu and Tri Dao. Mamba: Linear-time sequence modeling with selective state spaces. *arXiv preprint arXiv:2312.00752*, 2023. 1, 2, 4

[15] Albert Gu, Tri Dao, Stefano Ermon, Atri Rudra, and Christopher Ré. Hippo: Recurrent memory with optimal polynomial projections. *Advances in neural information processing systems*, 33:1474–1487, 2020. 2

[16] Albert Gu, Karan Goel, and Christopher Ré. Efficiently modeling long sequences with structured state spaces. *arXiv preprint arXiv:2111.00396*, 2021. 1, 2

[17] Albert Gu, Karan Goel, Ankit Gupta, and Christopher Ré. On the parameterization and initialization of diagonal state space models. *Advances in Neural Information Processing Systems*, 35:35971–35983, 2022. 2

[18] Yulan Guo, Hanyun Wang, Qingyong Hu, Hao Liu, Li Liu, and Mohammed Bennamoun. Deep learning for 3d point clouds: A survey. *IEEE transactions on pattern analysis and machine intelligence*, 43(12):4338–4364, 2020. 1

[19] Ankit Gupta, Albert Gu, and Jonathan Berant. Diagonal state spaces are as effective as structured state spaces. *Advances in Neural Information Processing Systems*, 35:22982–22994, 2022. 2

[20] Ramin Hasani, Mathias Lechner, Tsun-Hsuan Wang, Makram Chahine, Alexander Amini, and Daniela Rus. Liquid structural state-space models. *arXiv preprint arXiv:2209.12951*, 2022. 2

[21] Cheng-Yao Hong, Yu-Ying Chou, and Tyng-Luh Liu. Attention discriminant sampling for point clouds. In *Proceedings of the IEEE/CVF International Conference on Computer Vision*, pages 14429–14440, 2023. 7

[22] Xin Lai, Jianhui Liu, Li Jiang, Liwei Wang, Hengshuang Zhao, Shu Liu, Xiaojuan Qi, and Jiaya Jia. Stratified transformer for 3d point cloud segmentation. In *Proceedings of the IEEE/CVF Conference on Computer Vision and Pattern Recognition*, pages 8500–8509, 2022. 2

[23] Loic Landrieu and Martin Simonovsky. Large-scale point cloud semantic segmentation with superpoint graphs. In *Proceedings of the IEEE conference on computer vision and pattern recognition*, pages 4558–4567, 2018. 2

[24] Juho Lee, Yoonho Lee, Jungtaek Kim, Adam Kosiorek, Seungjin Choi, and Yee Whye Teh. Set transformer: A framework for attention-based permutation-invariant neural networks. In *International conference on machine learning*, pages 3744–3753. PMLR, 2019. 1

[25] Yangyan Li, Rui Bu, Mingchao Sun, Wei Wu, Xinhan Di, and Baoquan Chen. Pointcnn: Convolution on x-transformed points. *Advances in neural information processing systems*, 31, 2018. 2

[26] Dingkang Liang, Xin Zhou, Xinyu Wang, Xingkui Zhu, Wei Xu, Zhikang Zou, Xiaoqing Ye, and Xiang Bai. Pointmamba: A simple state space model for point cloud analysis. *arXiv preprint arXiv:2402.10739*, 2024. 1, 2, 4, 6, 7, 8

[27] Haotian Liu, Mu Cai, and Yong Jae Lee. Masked discrimination for self-supervised learning on point clouds. In *European Conference on Computer Vision*, pages 657–675. Springer, 2022. 7

[28] Yang Liu, Chen Chen, Can Wang, Xulin King, and Mengyuan Liu. Regress before construct: Regress autoencoder for point cloud self-supervised learning. In *Proceedings of the 31st ACM International Conference on Multimedia*, pages 1738–1749, 2023. 2

[29] Yue Liu, Yunjie Tian, Yuzhong Zhao, Hongtian Yu, Lingxi Xie, Yaowei Wang, Qixiang Ye, and Yunfan Liu. Vmamba:

Visual state space model. *arXiv preprint arXiv:2401.10166*, 2024. 1, 2

[30] Xu Ma, Can Qin, Haoxuan You, Haoxi Ran, and Yun Fu. Rethinking network design and local geometry in point cloud: A simple residual mlp framework. *arXiv preprint arXiv:2202.07123*, 2022. 7

[31] Andrew Ng, Michael Jordan, and Yair Weiss. On spectral clustering: Analysis and an algorithm. *Advances in neural information processing systems*, 14, 2001. 4

[32] Yatian Pang, Wenxiao Wang, Francis EH Tay, Wei Liu, Yonghong Tian, and Li Yuan. Masked autoencoders for point cloud self-supervised learning. In *European conference on computer vision*, pages 604–621. Springer, 2022. 1, 2, 5, 6, 7, 8

[33] Maciej Pióro, Kamil Ciebiera, Krystian Król, Jan Ludziejewski, and Sebastian Jaszczur. Moe-mamba: Efficient selective state space models with mixture of experts. *arXiv preprint arXiv:2401.04081*, 2024. 2

[34] Charles R Qi, Hao Su, Kaichun Mo, and Leonidas J Guibas. Pointnet: Deep learning on point sets for 3d classification and segmentation. In *Proceedings of the IEEE conference on computer vision and pattern recognition*, pages 652–660, 2017. 2, 6, 7

[35] Charles Ruizhongtai Qi, Li Yi, Hao Su, and Leonidas J Guibas. Pointnet++: Deep hierarchical feature learning on point sets in a metric space. *Advances in neural information processing systems*, 30, 2017. 1, 2, 6, 7

[36] Charles R Qi, Yin Zhou, Mahyar Najibi, Pei Sun, Khoa Vo, Boyang Deng, and Dragomir Anguelov. Offboard 3d object detection from point cloud sequences. In *Proceedings of the IEEE/CVF Conference on Computer Vision and Pattern Recognition*, pages 6134–6144, 2021. 1

[37] Guocheng Qian, Yuchen Li, Houwen Peng, Jinjie Mai, Hasan Hammoud, Mohamed Elhoseiny, and Bernard Ghanem. Pointnext: Revisiting pointnet++ with improved training and scaling strategies. *Advances in Neural Information Processing Systems*, 35:23192–23204, 2022. 7

[38] Martin Reuter, Franz-Erich Wolter, and Niklas Peinecke. Laplace-spectra as fingerprints for shape matching. In *Proceedings of the 2005 ACM symposium on Solid and physical modeling*, pages 101–106, 2005. 4

[39] Radu Bogdan Rusu and Steve Cousins. 3d is here: Point cloud library (pcl). In *2011 IEEE international conference on robotics and automation*, pages 1–4. IEEE, 2011. 1

[40] Jianbo Shi and Jitendra Malik. Normalized cuts and image segmentation. *IEEE Transactions on pattern analysis and machine intelligence*, 22(8):888–905, 2000. 4, 5

[41] Shaoshuai Shi, Xiaogang Wang, and Hongsheng Li. Pointrcnn: 3d object proposal generation and detection from point cloud. In *Proceedings of the IEEE/CVF conference on computer vision and pattern recognition*, pages 770–779, 2019. 1

[42] Yuan Tang, Xianzhi Li, Jinfeng Xu, Qiao Yu, Long Hu, Yixue Hao, and Min Chen. Point-lgmask: Local and global contexts embedding for point cloud pre-training with multi-ratio masking. *IEEE Transactions on Multimedia*, 2023. 2

[43] Yi Tay, Dara Bahri, Liu Yang, Donald Metzler, and Da-Cheng Juan. Sparse sinkhorn attention. In *International Conference on Machine Learning*, pages 9438–9447. PMLR, 2020. 1

[44] Mikaela Angelina Uy, Quang-Hieu Pham, Binh-Son Hua, Duc Thanh Nguyen, and Sai-Kit Yeung. Revisiting point cloud classification: A new benchmark dataset and classification model on real-world data. In *International Conference on Computer Vision (ICCV)*, 2019. 6, 8

[45] Mikaela Angelina Uy, Quang-Hieu Pham, Binh-Son Hua, Thanh Nguyen, and Sai-Kit Yeung. Revisiting point cloud classification: A new benchmark dataset and classification model on real-world data. In *Proceedings of the IEEE/CVF international conference on computer vision*, pages 1588–1597, 2019. 7

[46] Ashish Vaswani, Noam Shazeer, Niki Parmar, Jakob Uszkoreit, Llion Jones, Aidan N Gomez, Łukasz Kaiser, and Illia Polosukhin. Attention is all you need. *Advances in neural information processing systems*, 30, 2017. 2

[47] Hanchen Wang, Qi Liu, Xiangyu Yue, Joan Lasenby, and Matt J Kusner. Unsupervised point cloud pre-training via occlusion completion. In *Proceedings of the IEEE/CVF international conference on computer vision*, pages 9782–9792, 2021. 6

[48] Yue Wang, Yongbin Sun, Ziwei Liu, Sanjay E Sarma, Michael M Bronstein, and Justin M Solomon. Dynamic graph cnn for learning on point clouds. *ACM Transactions on Graphics (tog)*, 38(5):1–12, 2019. 6, 7

[49] Chengzhi Wu, Junwei Zheng, Julius Pfrommer, and Jürgen Beyerer. Attention-based point cloud edge sampling. In *Proceedings of the IEEE/CVF Conference on Computer Vision and Pattern Recognition*, pages 5333–5343, 2023. 6

[50] Xiaoyang Wu, Yixing Lao, Li Jiang, Xihui Liu, and Hengshuang Zhao. Point transformer v2: Grouped vector attention and partition-based pooling. *Advances in Neural Information Processing Systems*, 35:33330–33342, 2022. 2

[51] Xiaoyang Wu, Li Jiang, Peng-Shuai Wang, Zhijian Liu, Xihui Liu, Yu Qiao, Wanli Ouyang, Tong He, and Hengshuang Zhao. Point transformer v3: Simpler, faster, stronger. *arXiv preprint arXiv:2312.10035*, 2023. 2

[52] Zhirong Wu, Shuran Song, Aditya Khosla, Fisher Yu, Linguang Zhang, Xiaoou Tang, and Jianxiong Xiao. 3d shapenets: A deep representation for volumetric shapes. In *Proceedings of the IEEE conference on computer vision and pattern recognition*, pages 1912–1920, 2015. 6, 7, 8

[53] Li Yi, Vladimir G Kim, Duygu Ceylan, I-Chao Shen, Mengyan Yan, Hao Su, Cewu Lu, Qixing Huang, Alla Sheffer, and Leonidas Guibas. A scalable active framework for region annotation in 3d shape collections. *ACM Transactions on Graphics (ToG)*, 35(6):1–12, 2016. 6, 7

[54] Xumin Yu, Lulu Tang, Yongming Rao, Tiejun Huang, Jie Zhou, and Jiwen Lu. Point-bert: Pre-training 3d point cloud transformers with masked point modeling. In *Proceedings of the IEEE/CVF Conference on Computer Vision and Pattern Recognition*, pages 19313–19322, 2022. 1, 2, 6, 7

[55] Renrui Zhang, Ziyu Guo, Peng Gao, Rongyao Fang, Bin Zhao, Dong Wang, Yu Qiao, and Hongsheng Li. Point-m2ae: multi-scale masked autoencoders for hierarchical point cloud pre-training. *Advances in neural information processing systems*, 35:27061–27074, 2022. 1, 2, 5, 6, 7

[56] Renrui Zhang, Liuhui Wang, Yu Qiao, Peng Gao, and Hongsheng Li. Learning 3d representations from 2d pre-trained models via image-to-point masked autoencoders. In *Proceedings of the IEEE/CVF Conference on Computer Vision and Pattern Recognition*, pages 21769–21780, 2023. 2, 6, 7

[57] Tao Zhang, Xiangtai Li, Haobo Yuan, Shunping Ji, and Shuicheng Yan. Point could mamba: Point cloud learning via state space model. *arXiv preprint arXiv:2403.00762*, 2024. 1, 2, 4, 7

[58] Hengshuang Zhao, Li Jiang, Chi-Wing Fu, and Jiaya Jia. Pointweb: Enhancing local neighborhood features for point cloud processing. In *Proceedings of the IEEE/CVF conference on computer vision and pattern recognition*, pages 5565–5573, 2019. 2

[59] Hengshuang Zhao, Li Jiang, Jiaya Jia, Philip HS Torr, and Vladlen Koltun. Point transformer. In *Proceedings of the IEEE/CVF international conference on computer vision*, pages 16259–16268, 2021. 2

[60] Lianghui Zhu, Bencheng Liao, Qian Zhang, Xinlong Wang, Wenyu Liu, and Xinggang Wang. Vision mamba: Efficient visual representation learning with bidirectional state space model. *arXiv preprint arXiv:2401.09417*, 2024. 1, 2